

Differentiation between resonance Raman scattering and single vibrational level fluorescence 5100 cm^{-1} above the ${}^1B_{2u}$ origin in benzene vapor by means of excitation profiles

Paul A. Harmon and Sanford A. Asher^{a)}

Department of Chemistry, University of Pittsburgh, Pittsburgh, Pennsylvania 15260

(Received 9 February 1987; accepted 27 October 1987)

We have measured the absolute Raman scattering cross section of the $992\text{ cm}^{-1} a_{1g}$ ring breathing mode of benzene vapor in the 150 cm^{-1} region surrounding the $6_0^1 1_0^5$ vibronic transition to the ${}^1B_{2u}$ excited electronic state. We clearly observe emission directly from the resonant $6_0^1 1_0^5$ level, located $\sim 5100\text{ cm}^{-1}$ above the ${}^1B_{2u}$ origin. This Raman-like resonance emission is observed as an enhancement of the 992 cm^{-1} vibrational mode fundamental, as well as in the appearances of ν_1 overtones and the progression $2\nu_6 + n\nu_1$. Although the resonance emission from ${}^1B_{2u}$ vibronic levels has previously been denoted as "single vibrational level fluorescence" (SVLF), resonance fluorescence (RF), or hot luminescence (HL), we find by means of the analysis of the 992 cm^{-1} excitation profile that the resonance emission also contains a significant resonance Raman scattering (RRS) component. For excitation into the $6_0^1 1_0^5$ vibronic level of benzene vapor, the high density of background states within the molecule promotes processes such as dynamic intramolecular vibrational redistribution. These processes result in the intramolecular dephasing which determines the relative fractions of HL and RRS present in the emission from the ensemble of "isolated" molecules that give rise to the structured emission of vapor phase benzene. RRS derives from scattering from a superposition state while HL emission derives from an excited molecular eigenstate.

I. INTRODUCTION

The importance of a clear understanding of resonance emission and light scattering to spectroscopy has motivated numerous recent experimental and theoretical studies.¹⁻¹⁹ For an ensemble of molecules in a single well defined quantum level $|g\rangle$ of the ground electronic state which has an accessible rovibronic excited state $|m\rangle$, excitation in resonance with the absorption band of the $|m\rangle \leftarrow |g\rangle$ transition may result in the simultaneous observation of at least two spectrally different resonance emission line shapes.^{1,10,12} One dispersed emission line shape is associated with the Kramers-Heisenberg (KH) expressions for Raman scattering, and is Lorentzian with a bandwidth described by the damping parameters of only the initial $|g\rangle$ and final $|n\rangle$ states of the molecule. As the excitation frequency moves through the $|m\rangle \leftarrow |g\rangle$ absorption band, the center frequency of this Lorentzian band remains shifted by a constant frequency with respect to the laser excitation frequency. This shift corresponds to the frequency difference between the initial and final molecular states; for vibrational Raman scattering this would correspond to a vibrational frequency in the ground state. The other dispersed emission line shape will remain centered at the energy of the transition between the excited state $|m\rangle$ and the final state $|n\rangle$, regardless of the excitation frequency. This emission line shape has a bandwidth which reflects the damping parameters of the resonant excited molecular eigenstate $|m\rangle$, i.e., the bandwidth will be similar to that observed for the $|m\rangle \leftarrow |g\rangle$ absorption transition.

The central question is whether these spectrally differ-

ent resonance emission line shapes should be separately classified as resonance Raman scattering (RRS), resonance fluorescence (RF), or hot luminescence (HL), or as some combination of both. Different theoretical approaches choose to decompose the resonance emission into different sets of components each with a characteristic line shape. Unfortunately, similar terminologies are often used to describe the different sets. The terminology used here is adopted from that typically used in Raman spectroscopy, where the name (resonance) Raman scattering is given to that component of the resonance emission which remains displaced from the laser line by the frequency of the Raman active mode, while HL or RF refer to the component which remains centered at a constant energy. It should be noted that although the RRS and HL components are often treated as distinct scattering processes, Albrecht *et al.*¹³ have shown theoretically that when the initial and final states of the molecule differ, a third component exists, although its intensity is likely to be small compared to that of the RRS or HL component. Although this third component is generally ignored, its existence formally requires that RRS and HL be considered as components of one single resonance light scattering process. This third component will not be discussed further, as we will show below its intensity is indeed likely to be negligible relative to either the HL or the RRS component intensities in our experiments.

The classification of resonance emission into either the RRS or HL components as defined here depends upon the nature of the dephasing effects operative in the sample. Dephasing effects in Raman scattering must be described in terms of the coherence loss between those states within the molecule which are coupled by the radiation field; this coupling of states is simply the dynamic mixing of excited vi-

^{a)} Author to whom correspondence should be addressed.

bronic states into the ground electronic state wave function as described by time dependent perturbation theory. The resulting coherent superposition of ground and excited electronic state wave functions (the "superposition state") will oscillate in time with characteristic frequencies as long as the phase relationship between the superposed states is maintained. Pure dephasing processes are processes other than " T_1 " radiative and nonradiative decays that destroy the coherence between these superposed states; in gas phase experiments these processes are generally attributed to pseudoeelastic or phase perturbing collisions with the material bath. The point is that in the absence of pure dephasing effects, all molecules in the ensemble must scatter from the superposition state and the emission is described completely by the KH expressions; i.e., only the RRS component can occur. However, if pure dephasing effects are occurring, the superposition state in some molecules will be destroyed (dephased) which will populate isoenergetic molecular eigenstates. Subsequent emission will give rise to the HL component.

In this study, we examine whether the resonance emission observed from higher vibronic levels of the $^1B_{2u}$ electronic state of benzene vapor derives from the pure dephasing induced HL component or from the RRS component. Numerous $^1B_{2u}$ resonance emission studies of gas phase benzene have attempted to examine fundamental dynamical processes such as T_1 type energy relaxation.^{15,16,18,21-30} The discovery that the quantum yields of emission from $^1B_{2u}$ vibronic levels decrease dramatically with $\sim 3000\text{ cm}^{-1}$ of excess vibrational energy in the $^1B_{2u}$ manifold in what has since been called the "channel three" region of rapid nonradiative decay^{29,31} has led to a recent resurgence of studies of the resonance emission from these vibronic levels.^{16,18,23,25-28} In all of these studies the observed resonance emission has been called RF, HL, or single vibrational level fluorescence (SVLF). All previous attempts to experimentally differentiate between RRS and HL components (from any molecular resonance) have focused on resolving the difference in the emission line shapes. It has never been demonstrated, however, that the observed resonance emission from any $^1B_{2u}$ vibronic levels (from one photon excitation) is dominated by the HL line shape rather than the RRS line shape. This has been due to the experimental difficulty associated with distinguishing between the RRS and HL line shapes. While resonance emission is readily detected below the channel three threshold, the observed rovibronic absorption linewidths are generally far less than 1 cm^{-1} .³¹ The resolution required to differentiate a HL component line shape reflecting these absorption linewidths, from a RRS component line shape with an intrinsically narrower linewidth, is difficult to obtain in this UV spectral region. Although the rovibronic absorption linewidths approach several wave numbers above the channel three threshold, as described above, the resonance emission intensity becomes small.

In contrast to the previous methods of distinguishing between the RRS and HL components, we in this study directly characterize the dominant component(s) of the $^1B_{2u}$ resonance emission in the channel three region independent

of the emission line shapes. We accomplish this by taking advantage of the fact that in addition to having different emission line shapes, the excitation frequency dependence of the scattering amplitudes of the HL and RRS components must also be different. Since in RRS the coherence of the superposition between excited vibronic states and the ground state is maintained, the RRS amplitude is modeled by the familiar KH summation over the Raman amplitudes contributed by each of these superposed excited vibronic states, whether these excited states are resonant or nonresonant. Therefore, in the case where at least two excited states each give rise to significant Raman scattering amplitudes in a particular vibrational mode, interference between these amplitudes (the modulus squared of which is proportional to the Raman intensity) may occur as the excitation moves through resonance with one of these states (*vide infra*). However, if the emission from the resonant state is HL rather than RRS, no interference between resonant and nonresonant amplitudes can occur.

We probe the components of the $^1B_{2u}$ resonance emission by looking for evidence of interference effects between the Raman scattering amplitudes of the 992 cm^{-1} symmetric ring breathing vibrational mode contributed by resonant $^1B_{2u}$ vibronic levels and the nonresonant or "preresonance" Raman scattering amplitude active in this mode in the $^1B_{2u}$ transition energy region. This preresonance 992 cm^{-1} Raman scattering amplitude derives from much higher energy allowed electronic transitions^{32,33} and is independent of the vibronic absorption bands of the $^1B_{2u}$ state (*vide infra*). Indeed, with excitation only several wave numbers away from resonance with $^1B_{2u}$ vibronic absorption bands, the only significant intensity observed in any vibrational mode is the preresonant Raman intensity of the 992 cm^{-1} mode.

In Sec. IV of this paper we discuss our measurements of the 992 cm^{-1} mode Raman cross section as excitation approaches and moves through the $6_0^1 1_0^5$ $^1B_{2u}$ vibronic transition $\sim 5100\text{ cm}^{-1}$ above the $^1B_{2u}$ origin. We observe resonance emission from this vibronic level in the form of enhancement of the 992 cm^{-1} Raman fundamental intensity as well as the appearance of the overtones of the 992 cm^{-1} band and the progression $2\nu_6 + n\nu_1$. In Sec. V A we review expressions which describe resonant light scattering both in the presence and absence of pure dephasing processes, and demonstrate that the 992 cm^{-1} excitation profile through the $6_0^1 1_0^5$ region can reflect interference occurring between the 992 cm^{-1} resonant and nonresonant amplitudes. In Secs. V B and V C, we demonstrate that a Raman interference effect occurs in the 992 cm^{-1} excitation profile indicating that some portion of the observed 992 cm^{-1} mode resonance emission intensity (as well as all other observed vibrational progressions) from the pumped $^1B_{2u}$ vibrational levels must be RRS as described by the KH expression for Raman scattering. We then show the observed resonance emission has both HL and RRS contributions which are similar in magnitude.

In Sec. V D, we examine the nature of the pure dephasing process responsible for destroying the coherence between the 992 cm^{-1} resonant and nonresonant amplitudes in those molecules which contribute to the HL intensity.

Although these pure dephasing events have generally been attributed to intermolecular interactions we find that the pure dephasing in our experiments is an intramolecular event caused by the high density of background states within the molecule high in the ${}^1B_{2u}$ manifold. This high density of background states serves as an intramolecular bath for dephasing the states originally superposed by the incident field. These background states represent a large number of internal degrees of freedom which collectively dampen the time interval over which the coherence of the superposition state is maintained.

II. EXPERIMENTAL

The Raman spectrometer used has been described in detail elsewhere.³⁴ The excitation source is a Quanta Ray DCR2A Nd:YAG laser operated at 20 Hz and frequency doubled to pump a dye laser. UV light was generated by doubling the dye laser light and mixing it with the 1.06 μm fundamental of the YAG laser which produces continuously tunable excitation from 800 to 217 nm with a pulse duration of 6 ns and a spectral width of $\sim 0.25\text{ cm}^{-1}$. An ellipsoidal mirror was used to collect the scattered light. The scattered light was focused through a crystalline quartz wedge to randomize the polarization to avoid any polarization efficiency bias of the monochromator gratings. The light then passed into the slit of a modified SPEX Triplemate monochromator. A Princeton Applied Research OMA II intensified Reticon detector (model 1420) was used to detect the scattered light. Methane was used as the internal intensity standard for determining the benzene cross sections; the absolute Raman scattering cross section of the 2920 cm^{-1} symmetric carbon-hydrogen stretching mode of methane vapor has been determined between 600–200 nm.³⁵ The spectral widths observed derive from the spectrometer bandpass; thus, we determined the absolute Raman scattering cross sections from relative peak height measurements.

Benzene was obtained from Baker Chemical and used without further purification. Research grade methane was pumped through two successive bubblers containing liquid benzene to saturate the methane gas with benzene vapor. Raman spectra were obtained in an open flowing system at a controlled temperature of 24° ($\pm 0.5\text{ }^\circ\text{C}$). The gaseous mixture of ~ 80 Torr benzene and 680 Torr methane was passed through a 1 cm long cylindrical nozzle of 0.5 mm diameter, and then exhausted to a hood by a vacuum line. Excitation occurred 0.5 mm from the nozzle tip and the scattered light was collected at 90°. A nitrogen gas purge surrounded the sample and flowed uniformly about the long axis of the nozzle in order to surround the benzene-methane mixture with a noncombustible environment.

The short path length (0.25 mm) as well as the low absorption oscillator strength of the benzene vapor in the energy region studied here rendered self-absorption and optical saturation effects insignificant. The vibrational frequencies were calibrated by referencing to Raman spectra of acetonitrile under identical conditions. The quoted frequencies are estimated to be accurate to $\pm 5\text{ cm}^{-1}$. The 992 cm^{-1} band excitation profile data were obtained using a low resolution 600 groove/mm grating in the spectrograph stage

of the monochromator so that both the 992 cm^{-1} benzene band and the internal standard methane band at 2920 cm^{-1} were obtained simultaneously. A $\sim 75\text{ cm}^{-1}$ bandpass was used for the cross section measurements. Higher resolution spectra ($\sim 10\text{ cm}^{-1}$) were obtained with an 1800 groove/mm grating. Depolarization ratios were measured with a calibrated polacoat analyzer placed prior to the polarization scrambler.

III. NOTATION AND BAND ASSIGNMENTS

Absorption band assignments have been adapted from Parmenter *et al.*³⁶ as well as Stephenson, Radloff, and Rice.¹⁶ Band assignments use the notation introduced by Calloman, Dunn, and Mills.³⁷ For example, the notation $6_0^1 16_0^1 17_0^1$ indicates a transition in which only the ν_6 , ν_{16} , and ν_{17} vibrational modes are excited. In the ground state none of these vibrational modes are populated while in the upper electronic state one quanta of ν_6 , ν_{16} , and ν_{17} are excited. This notation can also be used to describe molecules in specific levels; $6^1 1^4$ would refer to an upper electronic state in which $\nu_6' = 1$ and $\nu_1' = 4$.

IV. RESULTS

Figure 1 shows a room temperature moderate resolution gas phase benzene absorption spectrum showing vibronic transitions to the electronically forbidden ${}^1B_{2u}$ electronic state. The vibronic activity observed in the ${}^1B_{2u} \leftarrow {}^1A_{1g}$ transition has been extensively characterized and will only briefly be reviewed here.^{15,16,36-40} In benzene (D_{6h} point group), electronic transitions are allowed to states of E_{1u} and A_{2u} symmetry. The oscillator strength observed for the forbidden ${}^1B_{2u} \leftarrow {}^1A_{1g}$ transition derives from the failure of the Condon approximation and the ${}^1B_{2u}$ state is Herzberg-Teller coupled to the ${}^1E_{1u}$ state. The ${}^1B_{2u}$ transition may therefore be induced by vibrations of a symmetry con-

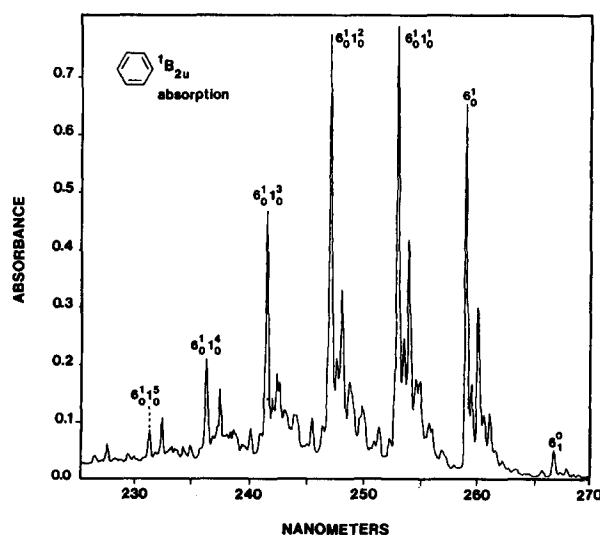


FIG. 1. Moderate resolution room temperature absorption spectrum of the ${}^1B_{2u} \leftarrow {}^1A_{1g}$ transition of gas phase benzene between 270–225 nm. The main progression in this vibronically induced transition is induced by the $\nu_6 e_{2g}$ vibration with ν_1 displaying Franck-Condon activity. This progression is labeled $6_0^1 1_0^5$.

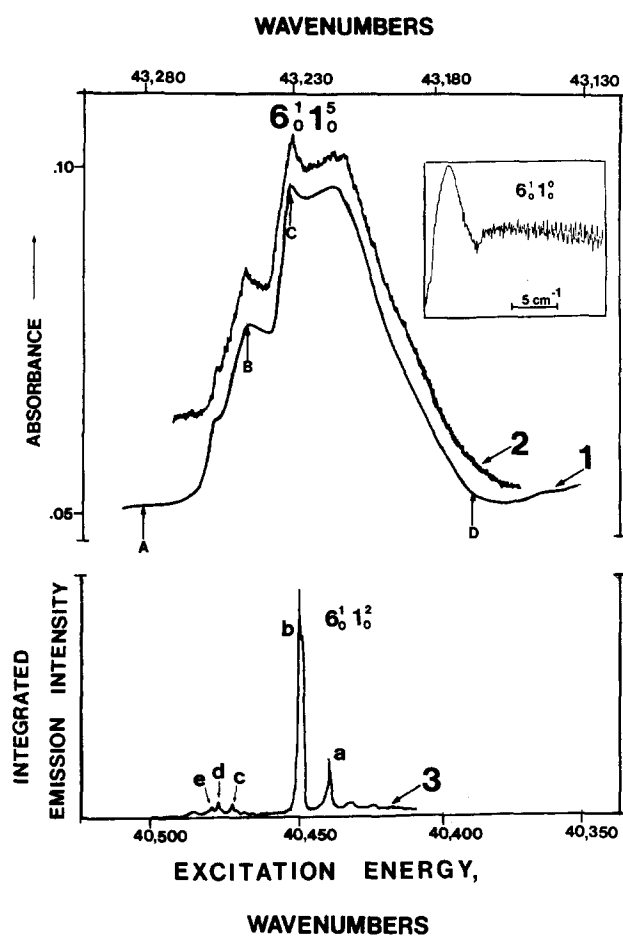


FIG. 2. The $2\text{--}3\text{ cm}^{-1}$ resolution absorption spectrum of the $6_0^1 1_0^5$ transition region between $43\,280$ and $43\,130\text{ cm}^{-1}$ (curve 1). Curve 2 is the transmitted power through the same region; upper abscissa scaling refers to curve 1 and 2. Curve 3 is the jet cooled fluorescence excitation profile through the $6_0^1 1_0^2$ transition adapted from Rice *et al.* (Ref. 16). Lower abscissa scales curve 3. Vibrational origins are assigned as (Ref. 15, 16, and 36): (a) $6_0^1 18_0^2 17_0^2 1_0^1 - 16_0^3 17_0^1 1_0^1$, (b) $6_0^1 1_0^2$, (c) $6_0^1 16_0^1 1_0^1$, $6_0^1 16_0^1 17_0^1 1_0^1$, (d) $6_0^1 16_0^1 17_0^1 1_0^1$, $6_0^1 4_0^1 10_0^1 1_0^1$, (e) $6_0^1 16_0^1 17_0^1 1_0^1$. Inset shows the first 20 cm^{-1} of the $6_0^1 1_0^5$ rovibronic absorption contour, adapted from Callomon *et al.* (Ref. 37).

tained in the cross product $B_{2U} \times E_{1u}$. Thus, only vibrations of e_{2g} symmetry or those combinations which contain e_{2g} character can induce transitions to the ${}^1B_{2u}$ state. The main progression in the ${}^1B_{2u}$ absorption spectrum is induced by the $\nu_6 e_{2g}$ vibration and displays a Franck–Condon progression in the $\nu_1 (a_{1g})$ 992 cm^{-1} ring breathing mode. This progression is labeled $6_0^1 1_0^2$ in Fig. 1. The broad structureless background absorption of ~ 0.04 absorbance units evident at higher energies is typical of absorption spectra of polyatomic molecules at high vibrational energies in excited electronic states, and presumably is due to sequence and hot band absorption as well as a larger homogeneous linewidth of the higher energy, shorter-lived states.

Curve 1 in Fig. 2 is a higher resolution ($2\text{--}3\text{ cm}^{-1}$) room temperature absorption spectrum of the $6_0^1 1_0^5$ transition region between $43\,280$ and $43\,130\text{ cm}^{-1}$. The well defined shoulder at $43\,240\text{ cm}^{-1}$ and the observation that the

structured absorption in curve 1 spans a 100 cm^{-1} interval indicates that additional vibronic absorption bands must overlap that of the $6_0^1 1_0^5$ transition. The detailed analysis of emission from the lower energy absorption members $6_0^1 1_0^n$ ($n = 1, 2$) by Parmenter *et al.*^{15,36} and later by Spears, Radloff, and Rice¹⁶ help us to easily assign these additional overlapping vibronic transitions. Curve 3 in Fig. 2 shows the jet-cooled fluorescence excitation profile through the $6_0^1 1_0^2$ region (lower energy axis, Fig. 2) adapted from that of Rice *et al.*¹⁶ The integrated fluorescence intensity vs excitation energy is plotted. The transition origins are easily resolved since only several rotational levels are populated. The transition origins in the $6_0^1 1_0^2$ region labeled a, b, c, d, and e in curve 3 of Fig. 2 are related to the underlying transitions in the $6_0^1 1_0^5$ region; those in the $6_0^1 1_0^5$ region derive simply from adding three quanta of ν_1 to the upper state of the transitions in $6_0^1 1_0^2$. The transition origins in the $6_0^1 1_0^2$ region are aligned below those in $6_0^1 1_0^5$ in order to facilitate comparison between the analogous transitions. For example, the vibronic origin labeled “b” in curve 3 corresponds to the $6_0^1 1_0^2$ origin; the $6_0^1 1_0^5$ origin would therefore be located at $\sim 43\,235\text{ cm}^{-1}$ near the observed absorption maximum.

At room temperature, many rotational levels are populated and the transition origins are not resolved in absorption because of overlapping rovibronic band shapes of the ~ 7 vibronic transitions occurring between $43\,280$ and $43\,180\text{ cm}^{-1}$. The rovibronic band shapes of ${}^1B_{2u} \leftarrow {}^1A_{1g}$ vibronic transitions are rather complex and have been characterized by Callomon *et al.*³⁷ Numerous transitions are known to exhibit absorption line shapes at room temperature characterized by a sharp high frequency edge $\sim 5\text{ cm}^{-1}$ to the blue of the transition origin followed by steadily decreasing absorption which can extend 60 cm^{-1} to lower energy. The inset in Fig. 2 illustrates the first 20 cm^{-1} of the $6_0^1 1_0^5$ rovibronic band shape. The $6_0^1 1_0^5$ band shape would be expected to be similar since the shape of the rovibronic absorption contour is influenced primarily by the Coriolis coefficients for ν_6 .³⁷ The sharp rise in absorption in curve 1 at $43\,235\text{ cm}^{-1}$ is, thus, the high frequency absorption edge of the $6_0^1 1_0^5$ transition, while the shoulder between $43\,250$ and $43\,235\text{ cm}^{-1}$ is assigned mainly to $6_0^1 16_0^1 17_0^1 1_0^4$ absorption but also contains contributions from overlapping $6_0^1 16_0^4 1_0^4$ and $6_0^1 4_0^1 10_0^1 1_0^1$ transitions. The additional absorption to the red of the $6_0^1 1_0^5$ maximum derives from the $6_0^1 18_0^2 1_0^3$ and the mixed $17_0^2 1_0^4 - 16_0^3 17_0^1 1_0^4$ transitions. It should be noted that the absorption features in curve 1 have a maximum molar absorptivity of only ~ 10 . Curve 2 in Fig. 2 was obtained by slowly scanning the laser excitation through a quartz cell containing 80 Torr benzene vapor and monitoring the transmitted power. This allows us to correlate our excitation energy with an exact location on the observed absorption envelope.

Figure 3 shows four representative Raman spectra A, B, C, and D obtained with excitation at the positions labeled A, B, C, and D (respectively) on the observed absorption features. Figure 3 shows changes in the 992 cm^{-1} band intensity relative to that of the methane internal standard at 2920 cm^{-1} as excitation is moved through the $6_0^1 1_0^5$ transition re-

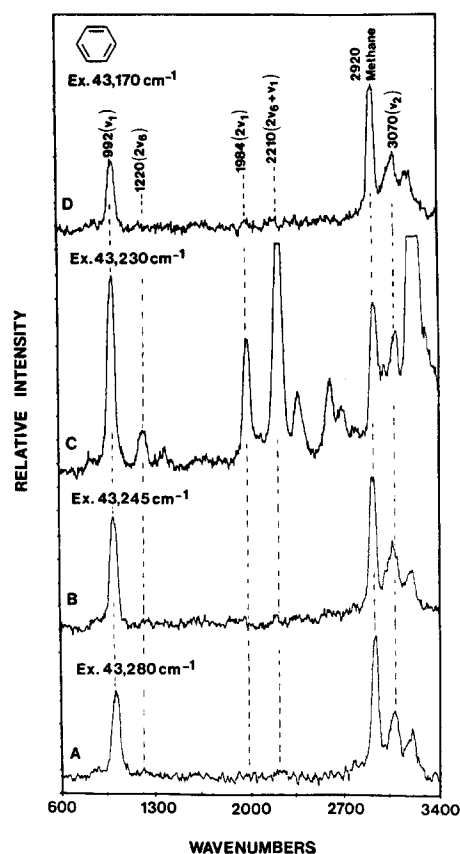


FIG. 3. Four representative Raman spectra A, B, C, and D obtained with excitation at the positions, labeled A, B, C, and D (respectively) of curve 1 of Fig. 2. Note the dramatic spectral changes in C, and changes in the ν_1 cross section relative to the methane internal intensity standard at 2920 cm^{-1} .

gion. The spectrum labeled A was obtained with $43\,280\text{ cm}^{-1}$ excitation which is not in resonance with any structured absorption feature. The only benzene modes with measurable intensity are the two totally symmetric modes; the ν_1 ring breathing mode at 992 cm^{-1} and ν_2 , the carbon-hydrogen stretching mode at 3060 cm^{-1} . As will be discussed further below, the 992 cm^{-1} intensity in spectrum A is the preresonance Raman intensity deriving from the allowed ${}^1E_{1u}$ and possibly ${}^1B_{1u}$ electronic states near 190 nm ; negligible intensity in the 992 cm^{-1} mode in spectrum A derives from ${}^1B_{2u}$ vibronic states. The band at 2920 cm^{-1} is the carbon-hydrogen stretching vibration of the methane standard. Spectrum B, although obtained in resonance with the absorption shoulder at $43\,245\text{ cm}^{-1}$, shows no activity in any of the expected vibrational progressions arising from emission or scattering from the levels $6^116^117^11^4$, $6^116^41^4$, or $6^14^110^11^4$. The only significant difference between A and B is a $\sim 20\%$ increase in the 992 cm^{-1} peak intensity in B relative to the methane band. Spectrum C, obtained with $43\,230\text{ cm}^{-1}$ excitation in resonance with $6^1_01^5_0$ absorption shows dramatic spectral changes; overtones of the 992 cm^{-1} band appear in addition to a progression in $2\nu_6 + n\nu_1$. Both of these features are characteristic of emission or scattering from an upper vibronic level in which both ν_1 and ν_6 are excited. The ν_1 progression results from a net $\Delta\nu_6 = 0$ for the Raman process, where $\Delta\nu_6 = +1(-1)$ in the upward

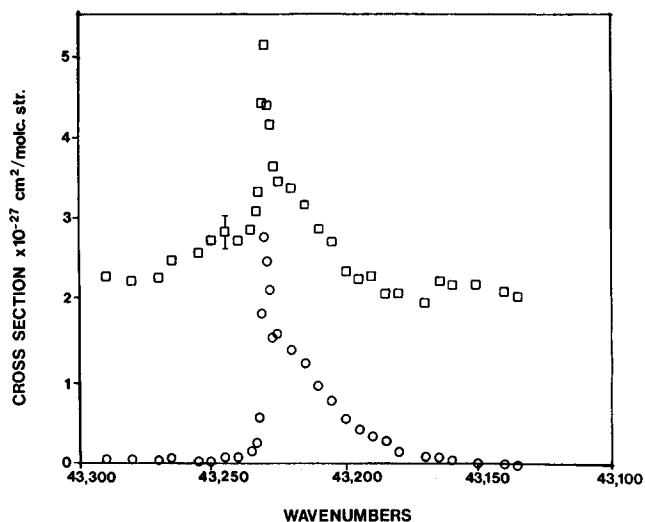


FIG. 4. Measured absolute Raman cross sections of the ν_1 992 cm^{-1} fundamental (squares) and the $2\nu_1$ overtone (open circles) through the 150 cm^{-1} region surrounding the $6^1_01^5_0$ vibronic absorption band. Error bar shown represents ± 2 standard deviations.

(downward) transition, while the $2\nu_6 + n\nu_1$ progression results from a net $\Delta\nu_6 = +2$, with ν_1 in both cases simply being Franck-Condon active. This type of overtone and combination scattering is typical for resonances with forbidden electronic transitions. A further increase in the 992 cm^{-1} fundamental intensity relative to that of the methane band should also be noted. It should be pointed out that spectrum C shows clearly, for the first time, that emission or scattering occurs directly from ${}^1B_{2u}$ vibronic levels well above the channel three threshold. Spectrum D results from $43\,170\text{ cm}^{-1}$ excitation which is to lower energy than structured absorption features. The spectrum has returned to the usual nonresonance appearance in the ${}^1B_{2u}$ region with Raman activity limited to only the two totally symmetric ν_1 and ν_2 modes.

The excitation profiles of the absolute scattering cross section of the 992 cm^{-1} ν_1 fundamental as well as the 1984 cm^{-1} $2\nu_1$ overtone are shown in Fig. 4 through the 150 cm^{-1} region surrounding the $6^1_01^5_0$ absorption band. Each data point is an average of two measurements, with a relative standard deviation of $\sim 5\%$. The ν_1 992 cm^{-1} intensity is seen to gradually increase from that observed off-resonance at $43\,280\text{ cm}^{-1}$ to that at $43\,245\text{ cm}^{-1}$ (see spectra A and B, Fig. 3). The sharply increased ν_1 cross section at $\sim 43\,230\text{ cm}^{-1}$ occurs in conjunction with the appearance of the ν_1 overtones and the $2\nu_6 + n\nu_1$ progression in spectrum C. The 1984 cm^{-1} overtone excitation profile rises sharply at this same excitation energy and has a "shape" similar to that of the expected $6^1_01^5_0$ rovibronic absorption contour, this indicates the dominance of this absorption band in contributing to ν_1 fundamental and overtone intensity. It is important to note that significant intensity changes occur for the 992 cm^{-1} fundamental without any concomitant increases in the overtone intensity. Figure 5, which shows the difference spectrum between spectra B and D of Fig. 3, demonstrates a selective intensity increase only for the 992 cm^{-1} mode fundamental.

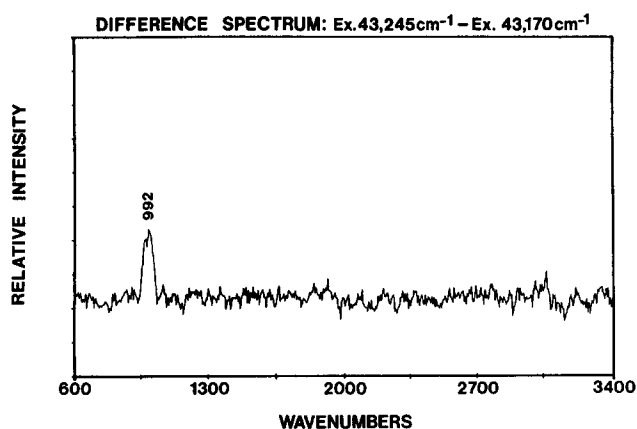


FIG. 5. Difference spectrum between spectrum B and spectrum D of Fig. 3, showing an intensity difference only for the 992 cm^{-1} fundamental.

Figure 6 shows the emission spectrum between 235–260 nm obtained with excitation at 43 230 cm^{-1} as in spectrum C of Fig. 3. The ν_1 overtones and the $2\nu_6 + n\nu_1$ progression members are observed throughout this region. An increased contribution of broad featureless emission is evident at longer wavelengths. The weaker $2\nu_{18} + n\nu_1$ and $2\nu_6 + 2\nu_{18} + n\nu_1$ progressions derive from the $6_0^1 18_0^2 1_0^3$ absorption band which overlaps the $6_0^1 1_0^5$ absorption maximum in the room temperature absorption spectrum. The two additional progressions, labeled A and B in Fig. 6, will be discussed below.

The $2\nu_6 + n\nu_1$ progression members display larger linewidths than that of the 992 cm^{-1} fundamental and overtones, which are instrumentally limited ($\sim 35 \text{ cm}^{-1}$ spectrometer bandpass in Fig. 6). This is expected due to the Fermi-resonance interactions between $\nu_6 + \nu_1$ and ν_8 .¹⁵ At our highest resolution of $\sim 10 \text{ cm}^{-1}$, we find the ν_1 progression linewidths are still less than our minimum spectrometer resolution. The progression members clearly do not derive from “relaxed” emission since the bands remain at the same displacement from the laser line over the entire 60 cm^{-1} excitation region where they appear. No spectral changes are observed when the total pressure is reduced from 760 to 70

Torr. The measured depolarization ratio of the 992 cm^{-1} $2\nu_1$ overtone and the $2\nu_6 + \nu_1$ combination band in Fig. 6 are 0.7 ± 0.1 and 0.9 ± 0.1 , while the ν_1 fundamental depolarization ratio with 43 230 cm^{-1} excitation is 0.3 ± 0.1 .

The relative intensities of the individual members of each progression in Fig. 6 are determined by their relative ν_1 Franck–Condon (FC) factors; the progression members differ only in the number of quanta of ν_1 in the final state. The relative intensity distribution within a progression deriving from a specific excited $^1B_{2u}$ vibronic level is then simply proportional to $\langle f|v \rangle^2$, where v is the number of quanta of ν_1 excited in the resonant $^1B_{2u}$ level and f is the number of quanta of ν_1 in the final state. The resonant levels have either three, four, or five quanta of ν_1 excited. These FC factors are readily calculated for ν_1 for excitation to the $^1B_{2u}$ state since the magnitude of the ring expansion along the ν_1 normal coordinate is well known.^{41,42} We use the simple harmonic oscillator recursion formulas reviewed by Mathies *et al.*⁴³ with a displacement of 1.7 dimensionless units in the excited state and take into account the change in frequency of the 992 cm^{-1} band upon excitation. Our results are essentially identical to those of Yoshihara *et al.*¹⁸ and Parmenter.¹⁵ Figure 7 shows the expected intensity distributions in progressions deriving from upper states where three, four, or five quanta of ν_1 are excited. A comparison of the observed Fig. 6 intensity distributions (uncorrected for monochromator efficiency) to the calculated distributions in Fig. 7 reveals that indeed the relative intensity distributions in the $2\nu_6 + n\nu_1$ and ν_1 progressions, except for the ν_1 fundamental, are best described by FC factors for an upper state in which five quanta of ν_1 are excited ($6^1 5$).

We find that although no vibrational progressions are observed from the states $6^1 16^1 17^1 1^4$, $6^1 16^4 1^4$, or $6^1 10^4 1^4$, which are responsible for the absorption shoulder $\sim 43 245 \text{ cm}^{-1}$, the integrated emission intensity observed at longer wavelengths does reflect this absorption shoulder. Figure 8 displays the “excitation profile” of the broad emission integrated between 260–280 nm. The excitation profile curve clearly reflects the spectral features observed in the absorption spectrum. We also attempted to observe the temporal relationship between the laser pulse excitation and the emis-

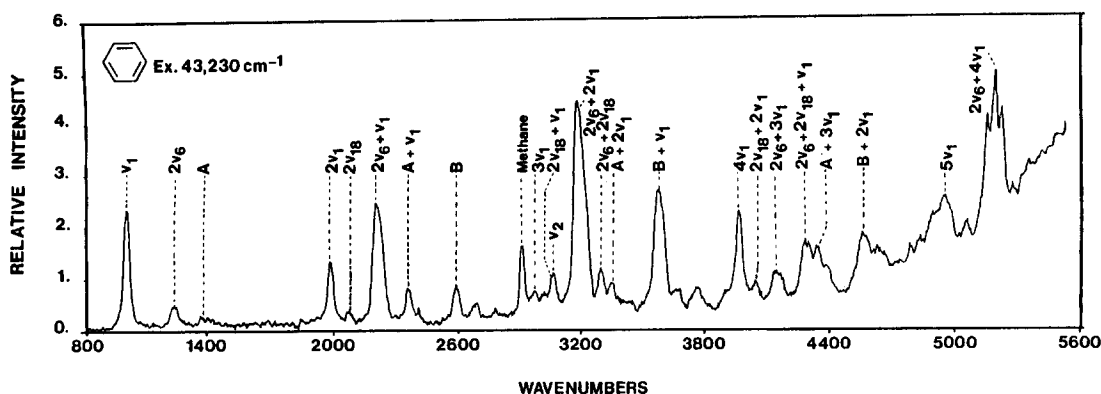


FIG. 6. Spectrum resulting from excitation at 43 230 cm^{-1} (cf. Fig. 3, spectrum C), showing all emission between 235–260 nm. Note an increasing contribution from “broader” emission can be seen in the rising base line at longer wavelengths. Experimental conditions identical to that of Fig. 3: 80 Torr benzene, 680 Torr methane.

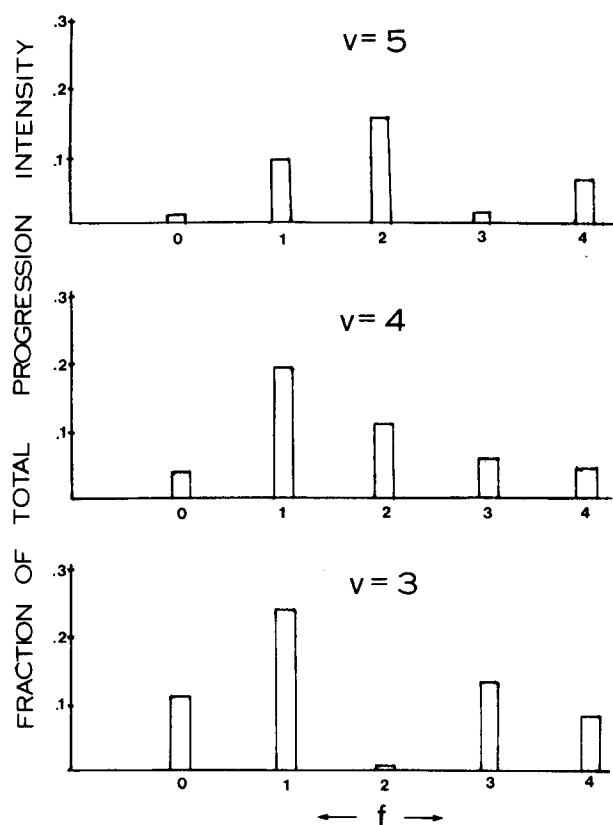


FIG. 7. Calculated relative intensity distributions within ν_1 Franck-Condon progressions which derive from upper states in which three, four, and five quanta of ν_1 have been excited. ν = number of quanta of ν_1 in upper state, while f = number of quanta of ν_1 in the final state.

sion from the resonant ${}^1B_{2u}$ vibronic levels by gating the Reticon detector on at times subsequent to the 6 ns excitation pulse. As anticipated, we can say only that the emission from these short lived states decays beyond our detection limit within 1 ns.

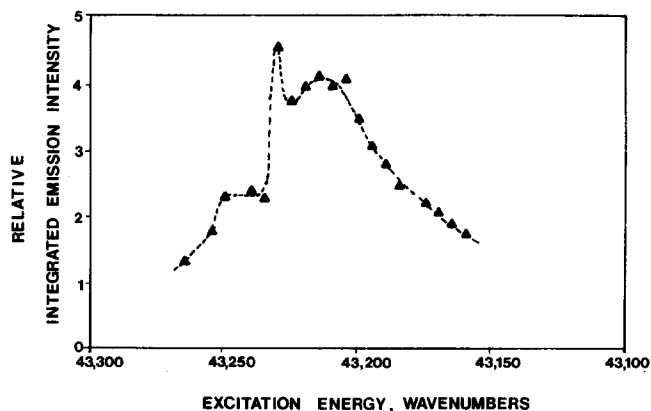


FIG. 8. "Excitation profile" of the broad emission between 260–280 nm. Solid triangles represent the relative integrated intensity of all emission between 260 and 280 nm as the excitation energy is varied through the $6_0^1 1_0^5$ absorption region. Conditions: 80 Torr benzene, 680 Torr methane.

V. DISCUSSION

At room temperature, benzene rotational levels up to $\sim J \cong 80$ are populated giving rise to several thousand different J, K initial quantum states which can undergo Raman transitions. At our resolution, the 992 cm^{-1} preresonance Raman intensity we measure in spectrum A of Fig. 3, as well as the additional 992 cm^{-1} resonance emission intensity apparent in spectrum C represents the integrated intensity of all $Q, P, R, S,$ and O branch rotational Raman scattering associated with the $\nu_1 = 1 - \nu_1 = 0$ Raman vibrational transition. In both cases the 992 cm^{-1} intensity will be dominated by Q branch scattering. For preresonance the Raman transition matrix elements (*vide infra*), which depend upon J and K , determine the relative contribution of a molecule to the integrated Raman intensity. However, with resonance excitation, selectivity also derives from the particular excitation frequency used since the 992 cm^{-1} resonance emission intensity derives mainly from molecules in those J and K initial states which have resonant ${}^1B_{2u}$ rovibronic transition energies.

The central question here is whether this enhancement of the ν_1 992 cm^{-1} mode preresonance Raman intensity and the spectral appearance of the ν_1 overtones and the $2\nu_6 + n\nu_1$ progression derives from the pure dephasing induced components of the resonant light scattering process or from RRS. In principle, these components may be differentiated by their emission line shapes as described above. The RRS component deriving from these rovibronic levels would remain displaced from the laser line by the frequency of the Raman scattered vibration throughout the entire $\sim 60 \text{ cm}^{-1}$ region in which the emission appears, and would exhibit a relatively narrow linewidth determined only by the initial and final ground state rovibronic linewidths. However, the HL component will also track with the laser line in our case due to the inhomogeneous site distribution of oscillator strength which derives from the rotational structure of these vibronic transitions. The HL emission linewidth, while characteristic of the resonant rovibronic levels, is too narrow to be diagnostic of the origin of the emission process; the $6_0^1 1_0^5$ rovibronic linewidths have been estimated by Callomon *et al.*³¹ using ultrahigh resolution absorption spectroscopy to be $2\text{--}3 \text{ cm}^{-1}$. We do not have sufficient resolution to discriminate between the RRS and pure dephasing induced emission linewidths; all components are simultaneously integrated in our experiments.

It should be noted that the measured depolarization ratios provide information on the resonance scattering time. An ensemble of benzene molecules excited in resonance within the x, y degenerate in plane $\pi \rightarrow \pi^*$ ${}^1B_{2u}$ vibronic transitions should show depolarization ratios of 0.125 for A -term scattering of the ν_1 fundamental and its overtones, and a depolarization ratio of 0.44 for the $2\nu_6 + \nu_1$ vibration, if the emission time scale is significantly shorter than the molecular rotation time. The measured depolarization ratios of $0.3 \pm 0.1, 0.7 \pm 0.1,$ and 0.9 ± 0.1 for resonance excitation for the $\nu_1, 2\nu_1,$ and $2\nu_6 + \nu_1$ bands indicate that the resonance emission (RRS and/or HL) time scale is on the order of a rotational period ($\sim 6 \text{ ps}$).

A. Review of Raman scattering theory and the utilization of the 992 cm⁻¹ mode excitation profile in determining the components of the ¹B_{2u} resonance emission intensity

If the incident field is considered to couple or superpose some initial state with electronic, vibrational, and rotational quantum numbers given by $|g\rangle = |g\rangle|i\rangle|JK\rangle$, and some excited electronic state $|m\rangle = |e\rangle|v\rangle|J'K'\rangle$, the dephasing decay parameters are defined as

$$\gamma_{g,m} = \frac{\gamma_g + \gamma_m}{2} + \gamma'_{g,m},$$

where $\gamma_{g,m}$ is the total coherence loss decay parameter (cm⁻¹), γ_g and γ_m are the T_1 population decay constants of the states $|g\rangle$ and $|m\rangle$, respectively, due to radiative and nonradiative relaxation, and $\gamma'_{g,m}$ is the pure dephasing coherence loss decay constant. As described in the Introduction, in the absence of pure dephasing processes ($\gamma'_{g,m} = 0$), only the RRS component can occur. The RRS intensity or cross section of the $n \leftarrow g$ molecular transition, where $|g\rangle$ and $|m\rangle$ are as defined above and $|n\rangle = |g\rangle|f\rangle|J''K''\rangle$, is given by the KH expressions as

$$\sigma_{n-g}(\text{RRS}) = K\nu_s^4 \sum_{\rho,\sigma} |\alpha_{\rho,\sigma}(\nu_0)|^2 F_{\text{RRS}}(\nu_s), \quad (1)$$

where $K = 2^3 \pi^2 / 3^2 (e^2/hc)^2$, ν_0 is the incident laser frequency, and ν_s is the frequency of the Raman scattered photon. $F_{\text{RRS}}(\nu_s)$ is the function which describes the dispersed emission line shape of the resonance Raman band. $\alpha_{\rho,\sigma}(\nu_0)$ is the ρ, σ ($\rho, \sigma = x, y, z$) component of the Raman scattering amplitude⁴⁴ contained in the molecular Raman polarizability tensor, which is given by the summation over all resonant and nonresonant intermediate states $|m\rangle$:

$$\alpha_{\rho,\sigma}(\nu_0) = \sum_m \left[\frac{\langle n|R_\sigma|m\rangle \langle m|R_\rho|g\rangle}{\nu_{m,g} - \nu_0 - i\gamma_{g,m}} + \frac{\langle n|R_\rho|m\rangle \langle m|R_\sigma|g\rangle}{\nu_{m,n} + \nu_0 - i\gamma_{g,m}} \right]. \quad (2)$$

R_σ is the electric dipole moment operator along the molecular coordinate σ . $\nu_{m,g} = \nu_m - \nu_g$, and $\nu_{m,n} = \nu_m - \nu_n$ are the upward and downward transition frequencies, respectively. The summation in Eq. (2) predicts that for each $\alpha_{\rho,\sigma}$ element of the polarizability tensor interference between resonant and nonresonant Raman amplitudes will occur in the case where both amplitudes contribute significantly.^{45,46}

Comparable preresonance and resonance 992 cm⁻¹ ν_1 amplitudes occur in the energy region of the ¹B_{2u} levels. The preresonant 992 cm⁻¹ mode Raman intensity has been shown to derive from higher energy electronic states^{32,33}; our recent vapor phase study of the 992 cm⁻¹ cross section between 514–217 nm (in which we explicitly avoided exact resonances with ¹B_{2u} vibronic absorption bands) gives a calculated 992 cm⁻¹ Raman cross section of 2.4×10^{-27} cm²/mol sr for an excitation energy of 43 280 cm⁻¹ which derives entirely from higher energy electronic states.³³ The in-plane polarized ¹E_{1u} and/or ¹B_{1u} electronic states around 190 nm dominate this 992 cm⁻¹ mode preresonance intensity with a small contribution from even deeper UV states. The measured 992 cm⁻¹ cross section at 43 280 cm⁻¹ of 2.3×10^{-27}

cm²/mol sr (spectrum A, Fig. 3) demonstrates that the ¹B_{2u} vibronic bands contribute negligibly except with exact resonance. Since the ¹B_{2u} transition as well as the ¹B_{1u} and ¹E_{1u} transitions are all in-plane polarized, $\alpha_{\rho,\sigma} = \alpha_{xx} = \alpha_{yy}$, $\alpha_{zz} = 0$ for both the resonant and preresonant 992 cm⁻¹ mode amplitudes, where x and y lie in the plane of the ring.

Both destructive and constructive interferences between the resonance and preresonance Raman amplitudes will occur because the sign of the denominator of the resonant ¹B_{2u} rovibronic term changes as excitation moves through the resonance. The sign of the preresonance Raman amplitude contributed by the higher energy electronic states remains fixed. Since the Raman intensity is proportional to the modulus squared of Eq. (2), as the excitation energy approaches and moves through ¹B_{2u} rovibronic absorption, the 992 cm⁻¹ mode excitation profile may show constructive followed by destructive interference or vice versa depending upon the initial signs of the numerators.

When $\gamma'_{i,m} \neq 0$, the coherence between those states superposed by the incident field is not maintained during the scattering process for all molecules in the ensemble, and the resonant light scattering amplitude cannot be expressed simply as in Eq. (2).¹⁻¹⁴ Albrecht *et al.*¹³ have derived the analogous expressions for Eqs. (1) and (2) in the presence of pure dephasing processes, where they explicitly consider only the resonant vibronic state contribution and assume the resonant term in Eq. (2) dominates. They find the resonance emission cross section per molecule, $\sigma_{n-g}^{\text{RE}}(\nu_0)$, to be¹³

$$\sigma_{n-g}^{\text{RE}}(\nu_0) = K\nu_s^4 \left| \frac{\langle n|R_\sigma|m\rangle \langle m|R_\rho|g\rangle}{\nu_{m,g} - \nu_0 - i\gamma_{g,m}} \right|^2 \times \left(F_{\text{RRS}}(\nu_s) + F_{\text{HL}}(\nu_s) \right) \times \left[\frac{2\gamma_{g,m}}{\gamma_m} - 1 \right] - \text{Third Term}. \quad (3)$$

The first term in Eq. (3) is exactly that given in Eqs. (1) and (2) when only the resonant term is considered significant. This is the RRS component. The second term in Eq. (3) is the HL, RF, or SVLF component and represents emission from molecules which have undergone dephasing before scattering of the photon. The function $F_{\text{HL}}(\nu_s)$ describes the HL emission line shape, while the factor $[2\gamma_{g,m}/\gamma_m - 1]$ is related to the probability that dephasing occurs before emission. This factor represents the ratio of molecules contributing to the HL vs RRS intensities, respectively, and reflects the relative magnitudes of the radiative and pure dephasing rates. Albrecht¹³ has shown that the intensity ratio of the third term in Eq. (3) to the RRS term will be approximately equal to the ratio of the ¹B_{2u} rovibronic lifetimes ($1/\gamma_{g,m}$) to the ground electronic state rovibronic lifetimes ($1/\gamma_{g,n}$). The ¹B_{2u} 6¹5 rovibronic lifetimes deduced from the ~2–3 cm⁻¹ linewidths are about 2.5 ps. Previous studies of collisionally induced rotational and vibrational relaxation rates show that the lifetimes of lower lying S₀ rovibronic levels, at 760 Torr, are completely dominated by “collision” induced rotational relaxation.⁴⁷⁻⁵¹ In the absence of collisions the lifetimes of low lying rovibronic levels of S₀ are expected to

be in the microsecond time regime.⁵⁰ Extrapolation to 760 Torr by considering previously measured rotational relaxation collisional cross sections^{24,48} results in S_0 rovibronic lifetime at least a factor of 10 longer than the ${}^1B_{2u}$ $6^1 1^5$ rovibronic levels. Therefore, the intensity of the third term in Eq. (3) is small relative to the RRS term. The third term is neglected in the following discussion.

An essential point is that nonresonant Raman amplitudes will add to the resonant scattering amplitude as in Eq. (2) only for those molecules contributing to the RRS component of Eq. (3). Therefore, interference in the 992 cm^{-1} mode excitation profile will only occur to the extent that a significant portion of the 992 cm^{-1} mode intensity enhancement (as well as ν_1 overtone and $2\nu_6 + n\nu_1$ band intensities) derives from the RRS component as described in Eq. (3) or Eqs. (1) and (2). If no interference is observed the pure dephasing induced components of Eq. (3) must dominate the observed resonance emission. Thus, we can utilize any interferences observed in the 992 cm^{-1} excitation profile to probe the origin of the ${}^1B_{2u}$ resonance emission intensity.

B. Demonstration of interference in the 992 cm^{-1} mode excitation profile

Any interferences observed in the 992 cm^{-1} mode excitation profile represent some ensemble average of interferences occurring in many individual rovibronic excitation profiles. The initial J, K distribution coupled with the benzene absorption selection rules of $\Delta J = 0, \pm 1$, and $\Delta K = 0, \pm 1$ give rise to $\sim 17\,000$ rotational transitions which contribute to the $6_0^1 1_0^5$ absorption band shape. With our pulsewidth of $\sim 0.25\text{ cm}^{-1}$, hundreds of rovibronic transitions are simultaneously resonant.

The most straightforward way to determine if the observed 992 cm^{-1} mode excitation profile reflects this interference is to compare the observed data to the 992 cm^{-1} mode profile which would result if the ${}^1B_{2u}$ resonance emission contained effectively no RRS component. This presumes that the increased probability of interaction with the photon for those molecules in resonance results only in population of ${}^1B_{2u}$ rovibronic levels. The rest of the ensemble merely gives rise to the 992 cm^{-1} mode preresonance Raman intensity. The expected 992 cm^{-1} excitation profile through the $6_0^1 1_0^5$ region would then simply be the sum of the preresonance Raman 992 cm^{-1} profile and the 992 cm^{-1} resonance emission profile. The preresonance 992 cm^{-1} Raman cross section excitation profile is essentially constant over the 200 cm^{-1} region of interest and has a value of $2.3 \times 10^{-27}\text{ cm}^2/\text{mol sr}$ as measured in spectrum A of Fig. 3. The resulting 992 cm^{-1} preresonance Raman excitation profile is given in Fig. 9 by the dashed curve labeled A.

The 992 cm^{-1} intensity deriving only from the resonance with ${}^1B_{2u}$ rovibronic levels can be calculated by considering the ${}^1B_{2u}$ rovibronic transition moments and the observed excitation frequency dependence of the intensity of bands which are observed only with exact resonance. If we assume the separation of electronic, vibrational, and rotational wave functions is valid, at any excitation energy the rotational matrix elements associated with any particular vibronic transition can be considered identical, and we can

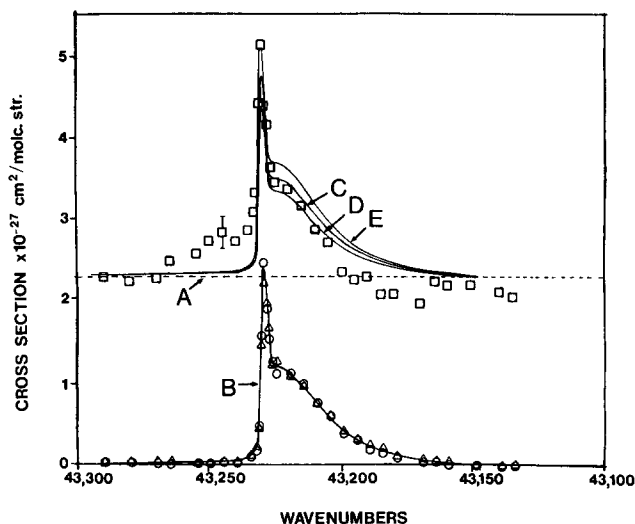


FIG. 9. Excitation profiles. The 992 cm^{-1} cross sections have been redisplayed from Fig. 4. The triangular data points in the lower portion of the figure correspond to the measured $2\nu_6 + \nu_1$ cross sections divided by 2.8. The circular data points represent the $2\nu_1$ cross sections displayed in Fig. 4 multiplied by 0.80. See the text for details. The 992 cm^{-1} preresonance Raman excitation profile is given by the dashed curve A and is a constant equal to $2.3 \times 10^{-27}\text{ cm}^2/\text{mol sr}$. The solid curve B represents the expected ν_1 resonance emission excitation profile. Curve C is curve A plus curve B, and is the 992 cm^{-1} profile expected if no RRS component exists in the 992 cm^{-1} resonance emission intensity. Curves D and E show a $\sim \pm 15\%$ variation in curve B similarly added to curve A.

treat only relative vibronic intensities. It is known from previous studies of ${}^1B_{2u}$ resonance emission that for upper levels of the type $6^1 X^1 Y^1 1^n$ or $6^1 X^2 1^n$, the dominant vibrational progressions in emission will be $6_{0,2} X_1 Y_1 1_n$ or $6_{0,2} X_2 1_n$, respectively, because the FC factors for simultaneous one quantum changes in X and Y , or a two quantum change in X are much smaller than those for a plus or minus one quantum change in ν_6 .¹⁵ Thus, the $6_0^1 1_0^5$ transition has the largest FC factors leading to resonance emission for the ν_1 fundamental and overtones. This is the origin of the similarity between the shape of the $2\nu_1$ excitation profile and the $6_0^1 1_0^5$ rovibronic absorption contour. It can easily be shown that¹⁵

$$\left[\frac{\langle 6_2 | Q_6 | 6^1 \rangle}{\langle 6_0 | Q_6 | 6^1 \rangle} \right]^2 = 3,$$

where 6^1 , 6_2 , and 6_0 are harmonic oscillator vibrational wave functions for the degenerate coordinate ν_6 . The intensity ratio of the $2\nu_6 + \nu_1$ band to the $2\nu_1$ band should be equal to this ratio of Franck-Condon factors, and the observed ratio is 2.8.

We can predict the excitation frequency dependence of the ν_1 992 cm^{-1} resonance emission cross section by measuring that of the $2\nu_6 + \nu_1$ band. The $2\nu_6 + \nu_1$ excitation profile and the ν_1 resonance emission profile will show identical shapes since all the excited vibronic states contributing to the absorption in Fig. 2 (except $17_0^2 1_0^4$) derive from vibrational transitions of the type $6_0^1 X_0^1 Y_0^1 1_0^n$ or $6_0^1 X_2^2 1_0^n$, and must, therefore, contribute proportionally to the resonance emission intensity of both the ν_1 and $2\nu_6 + \nu_1$ bands. Since the dominant progression characteristic of the level $17_2^2 1_2^4$, $(6_1 17_2 1_n)$,¹⁵ is not observed, its contribution to any other

progression must also be negligible. The 992 cm^{-1} resonance emission excitation profile can therefore be obtained by dividing the measured $2\nu_6 + \nu_1$ mode cross sections by our experimental value for the ν_6 FC ratio of 2.8. The resulting 992 cm^{-1} profile is given by the triangular data points in the lower portion of Fig. 9. In the same manner, the $2\nu_1$ cross sections (shown in the lower portion of Fig. 4) also check the consistency of the predicted shape of the ν_1 resonance emission excitation profile.

Initially, we scale the observed $2\nu_1$ cross sections by a constant (0.8) to obtain the best agreement with the triangular data points in Fig. 9. The result is given by the circular data points. Ideally, this constant should be equal to the ratio of the $2\nu_6 + \nu_1/2\nu_6 + 2\nu_1$ band intensities, which is observed to be 0.85. The agreement between these data is excellent. The solid curve labeled B in Fig. 9 drawn through the data points gives the expected ν_1 resonance emission profile through the $6_0^1 1_0^5$ transition region. The magnitude of curve B could be in error by as much as $\pm 10\%$ due to errors in the relative intensity measurements.

The ν_1 excitation profile which would be observed through the $6_0^1 1_0^5$ region, if the resonant 992 cm^{-1} emission given by curve B contains no RRS component, can now be obtained by simply adding curves A and B in Fig. 9. The resulting profile is given as curve C. The observed 992 cm^{-1} excitation profile clearly deviates significantly from curve C, as the predicted 992 cm^{-1} cross section is too small at higher energy excitation, and is too large at lower energy excitation. Curves D and E demonstrate that variation in the magnitude of curve B cannot reconcile the deviations between the observed and predicted 992 cm^{-1} excitation profiles.

The observed discrepancy is exactly what would be expected from resonance Raman interference between the pre-resonance and resonance ν_1 Raman amplitudes, as the data clearly reflect features associated with destructive and constructive interferences in the low and high energy wings of the excitation profile, respectively. The selective intensity change occurring in the 992 cm^{-1} mode fundamental, as given by the difference spectrum in Fig. 5, derives from this interference. If the 992 cm^{-1} intensity in Fig. 5 derived simply from an increased contribution of $992\text{ cm}^{-1} {}^1B_{2u}$ resonance emission in spectrum B, Fig. 3, then the $2\nu_6 + \nu_1$ band should also be apparent in Fig. 5 with an intensity ~ 3 times that of the ν_1 band. This is clearly not the case. Thus, some fraction of the molecules which are resonantly excited give rise to RRS where molecular eigenstates are not populated and interferences occur between resonance and pre-resonance contributions.

C. Modeling of interference effects

The interference in the 992 cm^{-1} mode excitation profile results from ensemble averaged interferences which derive from the many unresolvable rovibronic excitation profiles. By modeling this excitation profile we can extract parameters which will allow us to estimate the ratio of HL/RRS intensity from the ${}^1B_{2u}$ rovibronic levels. Curve A in Fig. 9 is easily modeled since the 992 cm^{-1} pre-resonance Raman cross section is simply a constant equal to $2.3 \times 10^{-27}\text{ cm}^2/\text{mol sr}$ as described above. The value for the

amplitude $\alpha_{\rho,\sigma} = \alpha_{xx,yy}$ can be easily determined from Eq. (2) when we neglect the damping parameter because it is negligibly small relative to the energy differences $\nu_{m,g} - \nu_0$ or $\nu_{m,n} + \nu_0$ and thus has a negligible imaginary component. Substitution of the pre-resonance 992 cm^{-1} cross section into Eq. (1) along with the appropriate constants give a value of $9.8 \times 10^{-22}\text{ cm}^3/\text{molecule}$ for the pre-resonance amplitude.

The modeling of curve B in Fig. 9 is more complex. We begin with Eq. (2) and include only the resonant term since the summation over $|m\rangle$ here concerns only the rovibronic levels giving rise to the absorption in Fig. 2. We also consider the contribution of cross terms between these rovibronic levels negligible compared to the resonant moduli squared. The cross terms which arise because a molecule in a given initial state $|g\rangle = |g\rangle|i\rangle|JK\rangle$ has access to more than one upper rovibronic state via the benzene absorption selection rules, are neglected because the likely energy gaps between levels accessible by a molecule in an initial J, K quantum state are large compared to the damping constant $i\gamma_{g,m}$. Indeed, even if these cross terms contribute it will only lead to a small error in the value of F (*vide infra*), which will not alter any of the conclusions.

We can thus model the distribution of rovibronic transition energies giving rise to curve B as a simple inhomogeneous distribution. Since we know the number of transitions is large and we do not resolve them in our measurements, we model curve B by convolving a transition energy distribution function with the Lorentzian excitation profile molecular response function as given by Eqs. (2) and (3). Thus, the 992 cm^{-1} resonance emission cross section, $\sigma^{\text{RE}}(\nu_0)$ can be written as

$$\sigma^{\text{RE}}(\nu_0) = K\nu_s^4 F^2 \int G(\nu_i) \left[\frac{1}{\nu_i - \nu_0 - i\gamma_i} \right]^2 d\nu_i, \quad (4)$$

where K , ν_s , and ν_0 are as previously defined. $G(\nu_i)$ is the distribution function which has the shape expected for the $6_0^1 1_0^5$ rovibronic absorption contour and is normalized to unit area. The expression in brackets gives the Lorentzian response about the resonant frequency ν_i . γ_i is the total coherence loss decay parameter associated with each transition. In this model $F = \langle n|R_\sigma|m\rangle \langle m|R_\rho|g\rangle$ and represents the rotational, vibrational, and electronic matrix elements associated with the $\nu_1 = 1 \leftarrow \nu_1 = 0$ Raman vibrational transition averaged over all orientations as well as all initial and final states of the room temperature vapor phase sample. Since the $6_0^1 1_0^5$ rovibronic transitions dominate these matrix elements, we take γ_i here to be the $6_0^1 1_0^5$ rovibronic linewidth measured by Callomon ($\gamma_i = 2.5\text{ cm}^{-1}$). We fit Eq. (4) to curve B of Fig. 9 by varying the shape of the distribution function and the magnitude of F . The fitted value of F is $2.5 \times 10^{-21}\text{ cm}^2$.

The value of the Raman matrix elements monitored by parameter F may be quantitatively compared to that calculated from the absorption spectrum in Fig. 2. The integrated oscillator strength of the structured absorption in Fig. 2 is $\sim 2 \times 10^{-6}$ giving a value of $3 \times 10^{-22}\text{ cm}^2$ for $|\langle g|R_\sigma|m\rangle|^2$. The value of the factor

$$\left[\langle g|R_\sigma|m\rangle \right]^2 \bigg/ \frac{\langle i|v\rangle \langle JK|J'K'\rangle}{\langle v|f\rangle \langle J'K'|J'K''\rangle} \quad (5)$$

(again, averaged over all orientations and relevant quantum levels) should be equal to the value we find for F . Since the maximum in the rotational distribution at room temperature is at $J \approx 24$, the value of the matrix elements $\langle JK | J'K' \rangle$ will not be dramatically different than the value of $\langle J'K' | J''K'' \rangle$ for the majority of the ensemble. We therefore take the average value of the ratio of these matrix elements as simply being equal to unity in Eq. (5). The vibrational overlap integrals refer only to the 992 cm^{-1} mode with $i = 0, f = 1$, and $v = 3, 4$, and 5 quanta. Since the absorption in Fig. 2 is dominated by vibronic levels with $v = 4$ and 5 , the value for the FC factors $\langle i|v\rangle/\langle v|f\rangle$ lie between 0.25 and 0.16 (see Fig. 7) given all possible contributions to the absorption of levels with $v = 4$ and 5 . The calculated value of Eq. (5) lies between 1.2 and $2.0 \times 10^{-21} \text{ cm}^2$, which is satisfying close to our value of $F = 2.5 \times 10^{-21} \text{ cm}^2$.

We utilize the $G(\nu_i)$ and F parameters and Eq. (4) to model interferences in the 992 cm^{-1} mode excitation profile $\sigma(\nu_0)$:

$$\sigma(\nu_0) = K\nu_s^4 F^2 \int G(\nu_i) \left[\left| \frac{A}{\nu_i - \nu_0 - i\gamma_i} + 9.8 \times 10^{-22} \text{ cm}^3 \right|^2 + \left| \frac{B}{\nu_i - \nu_0 - i\gamma_i} \right|^2 \right] d\nu_i, \quad (6)$$

where all parameters and the distribution function are fixed from the modeling of curve B via Eq. (4). The molecular response function is given by the expression inside the brackets is no longer simply Lorentzian; however, if the value of the preresonance 992 cm^{-1} amplitude is set equal to zero the expression in brackets becomes Lorentzian. The parameters A and B monitor the fraction of emission amplitude which gives rise to RRS or HL, respectively. $A^2 + B^2$ must equal unity in Eq. (6). The ratio B^2/A^2 represents the ratio of HL/RRS intensity from the ${}^1B_{2u}$ vibronic levels and is the counterpart of the quantity $[2\gamma_{g,m}/\gamma_m - 1]$ in Eq. (3). The first term inside the brackets in Eq. (6) therefore represents those molecules scattering from the superposition state; the preresonance Raman amplitude and the ${}^1B_{2u}$ resonance Raman amplitude are added before taking the modulus squared. This term gives rise to the interference phenomena described previously. The second term which is always Lorentzian derives from different molecules where pure dephasing has destroyed the superposition state before emission. If $A = 0$ and $B = 1$ in Eq. (6), there is no interference, no RRS component exists, and curve C in Fig. 9 is obtained. We simply allow the parameters A and B to vary within the limits described above to obtain the best fit (by inspection) to be observed data.

Incorporation of such interference effects dramatically improves the agreement between the predicted and observed 992 cm^{-1} mode excitation profiles. The best agreement is obtained with $A \approx B \approx 0.7$. The resulting calculated profile is shown in Fig. 10 agrees closely with the observed data and demonstrates the 992 cm^{-1} mode excitation profile derives from ensemble averaged interferences occurring in many unresolved rovibronic excitation profiles. The relative values of A and B suggest that the integrated intensities of the RRS and HL components from the ${}^1B_{2u}$ rovibronic levels are similar in magnitude.

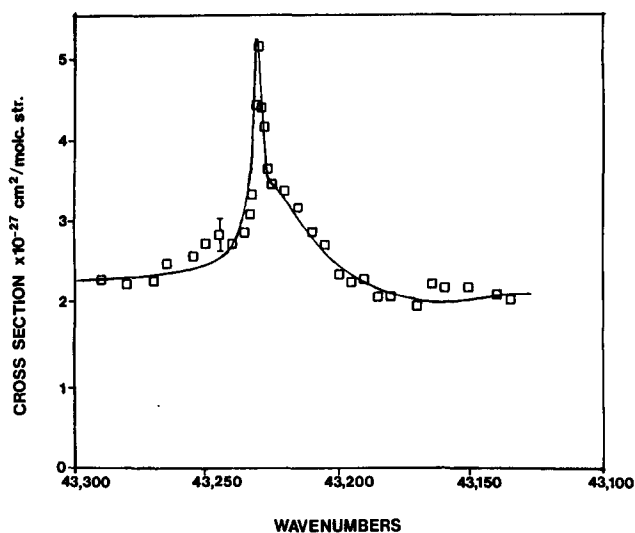


FIG. 10. Solid curve gives "best fit" (by inspection) to the data using Eq. (6) and allows for both RRS as well as HL from the resonant ${}^1B_{2u}$ rovibronic levels. The improved agreement between this curve and the data relative to that for curve C in Fig. 9 derives from the interference between the ${}^1B_{2u}$ RRS component and the higher energy E_{1u} or B_{1u} state Raman preresonance amplitudes.

D. The nature of the pure dephasing process

The observation of both the RRS and HL components of the resonant light scattering process requires a pure dephasing process with a rate similar to that of the T_1 decay rate. As described in the Introduction, pure dephasing processes in vapor phase experiments have generally been attributed to pseudoeelastic collisions. To determine if this was the pure dephasing mechanism operative in this study, we measured the 992 cm^{-1} ν_1 fundamental and 1984 cm^{-1} overtone cross sections with a methane/benzene total pressure of 70 Torr. We find that the shape and magnitude of the resulting ν_1 and $2\nu_1$ excitation profiles are identical within experimental error to those displayed in Fig. 4 which were obtained at a total pressure of 760 Torr. The observation that the resonance emission cross sections do not increase as the pressure is reduced would imply that collisional processes contribute negligibly to the total dephasing linewidth $\gamma_{mg} = (\gamma_m + \gamma_g/2) + \gamma'_{mg}$, and further that the relative magnitudes of both γ_m and γ'_{mg} must remain unchanged. However, this analysis is complicated in our case because the absorption is strongly inhomogeneously broadened. In the previous two sections, however, we showed that the ν_1 992 cm^{-1} mode excitation profile was sensitive to the relative amounts of HL and RRS deriving from the multitude of resonant ${}^1B_{2u}$ rovibronic levels due to the interference of the RRS component with the 992 cm^{-1} preresonant Raman contributions. The fact that the 992 cm^{-1} mode excitation profile is unchanged at 70 or 760 Torr indicates the ratio of HL/RRS intensity deriving from the ${}^1B_{2u}$ levels is not a function of any intermolecular collisional processes.

This lack of pressure dependence of the ratio of the HL to RRS intensities is consistent with the recent study of collisional broadening effects on the linewidths of individual rovibronic absorption transitions measured by Riedle *et al.*,²⁴

who measured a collisional broadening parameter of 15 MHz/Torr. The rovibronic linewidth reflects the total coherence loss decay parameter $\gamma_{g,m}$ and must include the contribution from pure dephasing. Even at 760 Torr, this broadening parameter gives rise to a $\sim 0.2 \text{ cm}^{-1}$ contribution to the rovibronic linewidth from intermolecular interactions; this is small compared to the $\sim 2.5 \text{ cm}^{-1}$ $6^1_0 1^5_0$ rovibronic linewidths estimated by Callomon. Since the T_1 contribution to these linewidths is only 0.2 cm^{-1} (*vide infra*), this suggests that a pressure independent intramolecular process determines the observed ratio of HL/RRS intensity from these $^1B_{2u}$ levels. Indeed, we believe that the pure dephasing process responsible for the ratio of HL/RRS intensity we observe here is the same process which gives rise to the well established intramolecular line broadening of higher energy $^1B_{2u} \leftarrow A_{1g}$ vibronic transitions.²¹⁻³¹ Although this line broadening has been suspected for some time of being due to intramolecular vibrational redistribution (IVR),^{21,25,27} this has only recently been confirmed by the chemical timing experiments of Parmenter *et al.*²⁶ They showed that a dynamic IVR process exists in the higher energy $^1B_{2u}$ vibronic levels studied and that the lifetimes inferred from rovibronic absorption linewidth measurements correspond to IVR rather than T_1 lifetimes.

The description of IVR has appeared numerous times in the literature,⁵²⁻⁵⁴ and we present here only a brief description aimed at developing a qualitative understanding of the IVR process as a pure-dephasing mechanism. The essential elements are presented in Fig. 11. The state $|s\rangle$ and its neighboring field of states $|l\rangle$ are zero-order (harmonic basis sets) $^1B_{2u}$ vibrational or rovibrational levels. The $|s\rangle$ state is treated separately as it is the only state with significant FC factors to a thermal level in the ground state and is therefore prominent in absorption while the $|l\rangle$ states represent "dark" background states. In our case, the $|s\rangle$ state would correspond to $6^1_0 1^5_0$ rovibronic levels. Anharmonic and/or vibronic couplings (V_{sl}, V_{ll}) mix these zero-order levels to produce the true molecular eigenstates $|j\rangle$. Each $|j\rangle$ level can then be viewed as some mixture of $|s\rangle$ and various $|l\rangle$ zero-order states. The distribution of $|s\rangle$ character into the $|j\rangle$ molecular eigenstates is represented by the heavy shading in Fig. 11.

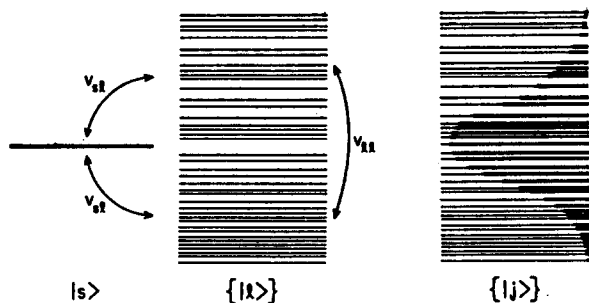


FIG. 11. Schematic diagram of the conventional state mixing model for IVR. The zero-order levels $\{|l\rangle\}$ and $|s\rangle$ are mixed through the anharmonic or vibronic coupling matrix elements $V_{sl} \approx V_{ll}$. The resulting dispersion of $|s\rangle$ character into the $\{|j\rangle\}$ true molecular eigenstates is depicted by the heavier shading in the $\{|j\rangle\}$ manifold. Adapted from Parmenter *et al.* (Ref. 53).

IVR, or a time evolution of the molecular vibrational identity, can occur when the coherence width of the excitation is wide enough (or the $|j\rangle$ state density high enough) such that a considerable portion of the levels containing the zero-order $|s\rangle$ state character are coherently excited. The description of the coherent superposition of the $|j\rangle$ molecular eigenstates at "short times" closely resembles that of the single zero-order state $|s\rangle$.^{53,54} A more complicated vibrational identity will evolve in time as this coherent superposition dephases due to the V_{ll} and V_{sl} couplings, populating the $|j\rangle$ molecular eigenstates. The IVR decay time corresponds to how long the coherent superposition state survives before molecular eigenstates are populated. IVR will cause emission, which at short times is structured and characteristic only of the $|s\rangle$ vibrational identity, to become increasingly broad at longer times reflecting not only the $|s\rangle$ but also the many $|l\rangle$ zero-order vibrational identities which define the $|j\rangle$ molecular eigenstates.

The essential point is that IVR is intimately involved in the time evolution (dephasing) of a superposition state into a molecular eigenstate. Since in the more rigorous case the description of this superposition state (in the IVR terminology, the coherent superposition of $|j\rangle$ molecular eigenstates at "short times") must include contributions from resonant as well as nonresonant vibronic states, IVR dephasing actually serves to limit the time interval over which Raman amplitudes contributed by resonant and nonresonant vibronic states can interfere. The summation over m in Eq. (2) is valid for those molecules which scatter before IVR; these molecules will have 992 cm^{-1} mode resonance Raman amplitudes which reflect contributions from both the resonant $^1B_{2u}$ vibronic levels as well as the higher energy $^1E_{1u}$ and $^1B_{1u}$ electronic states. Interference will exist in the 992 cm^{-1} mode excitation profiles of these molecules. After IVR, $^1B_{2u}$ molecular eigenstates are populated. 992 cm^{-1} resonance emission can still occur due to the dispersion of $|s\rangle$ ($6^1_0 1^5_0$)

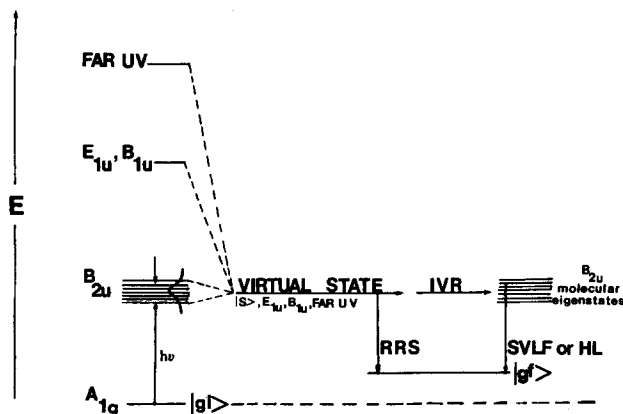


FIG. 12. Schematic diagram of RRS, IVR, and HL. Closely spaced horizontal lines represent $^1B_{2u}$ molecular eigenstates as in Fig. 11, solid curve represents dispersion of $|s\rangle$ character into these levels. The laser excitation coherence width is considered to span this dispersion of $|s\rangle$ character. The superposition or virtual state, which gives rise to RRS component and interference effects contains contributions from resonant and preresonant states. IVR dephases the superposition state and populates the $^1B_{2u}$ $|j\rangle$ molecular eigenstates; emission from these eigenstates is HL or SVLF.

vibrational character in the $|j\rangle$ molecular eigenstates as given in Fig. 11. However, the 992 cm^{-1} mode amplitude from these molecules will not reflect any contribution from higher energy electronic states, and thus, represents the HL component. *Dynamic IVR serves as the pure dephasing process which destroys the superposition state from which RRS occurs and populates the ${}^1B_{2u}$ molecular eigenstates responsible for HL.* Figure 12 schematically represents the temporal relation described between RRS, IVR, and HL (SVLF).

It should be pointed out that Parmenter's²⁶ study of IVR in benzene ${}^1B_{2u}$ vibronic levels has not been extended to levels as high above the ${}^1B_{2u}$ origin as 6^11^5 . The occurrence of IVR in 6^11^5 is certain since Parmenter has demonstrated IVR in 6^11^3 using a YAG pumped dye laser system with coherence characteristics similar to our own, and because of the increased density of states in the 6^11^5 energy region compared to the 6^11^3 region. We also observe an increasing amount of broad, structureless emission at longer wavelengths suggestive of emission from many $|j\rangle$ molecular eigenstates populated via IVR; this can be seen in Fig. 6 as the rising base line toward large displacements from the laser line. Additionally, the fact that the excitation profile of the (integrated) intensity of this broad emission follows the shape of the observed absorption contour (see Figs. 2 and 8), while we observe little or no emission directly from the vibronic levels responsible for the absorption shoulder at $\sim 43\,240\text{ cm}^{-1}$, suggests that a more "efficient" IVR occurs for these levels. It is also interesting to note that the progressions labeled A and B in Fig. 6, which are only observed with excitation energies less than $43\,230\text{ cm}^{-1}$, seem to be satisfactorily assigned only as progressions expected from those vibronic levels responsible for the absorption shoulder at $43\,240\text{ cm}^{-1}$. An increased intensity in these modes could be explained by the occurrence of a dynamic IVR process in the 6^11^5 rovibronic levels which populates these overlapping rovibronic levels; although it is not apparent why the intensity of these progressions should be greater than is observed with excitation directly in resonance with these vibronic levels.

The ratio of HL/RRS intensity observed from these ${}^1B_{2u}$ rovibronic levels is consistent with Eq. (3) and the measured rovibronic linewidths and the T_1 lifetimes of these levels. The ratio of HL/RRS intensity predicted from Eq. (3) is $(2\gamma_{g,m}/\gamma_m) - 1 \approx 2\gamma'_{g,m}/\gamma_m$, if as expected $\gamma_g \ll \gamma_m$. The T_1 lifetimes of the molecular eigenstates in the 6^11^5 region have been measured by Yoshihara *et al.*,²¹ who recorded the time resolved decay of the integrated intensity of the predominantly featureless emission near 290 nm resulting from a several picosecond laser pulse resonant with the $6^1_01^5_0$ transition (recall, this is the broad emission we integrated to obtain Fig. 8). They observe an exponential decay of ~ 30 ps, which gives $\gamma_m \approx 0.2\text{ cm}^{-1}$. The $2\text{--}3\text{ cm}^{-1}$ rovibronic linewidth measurement of Callomon for $6^1_01^5_0$ transitions gives $\gamma_{g,m} = 2\text{--}3\text{ cm}^{-1}$ which yields $\gamma'_{g,m} \approx 2\text{--}3\text{ cm}^{-1}$, corresponding to a $2\text{--}3$ ps IVR lifetime. Thus, the value of $2\gamma'_{g,m}/\gamma_m$ will be between 20 and 30.

Initially, this predicted HL/RRS intensity ratio seems to contradict our excitation profile result which suggests the HL and RRS components have similar integrated intensities. However, Eq. (3) intrinsically assumes that during the

T_1 30 ps decay of the $|j\rangle$ molecular eigenstates, emission into the 992 cm^{-1} band occurs with the same efficiency as it does in the $2\text{--}3$ ps prior to IVR. This is simply not the case when a dynamic IVR process exists, as described above. In the case of resonance with 6^11^5 rovibronic levels, emission or scattering before IVR will occur primarily in the ν_1 fundamental and overtones as well as the $2\nu_6 + n\nu_1$ progression, while after IVR, the emission is distributed into many vibrational progressions characteristic of the number of coupled dark (vibrational) states N . This serves to reduce the amount of HL in the 992 cm^{-1} mode predicted via Eq. (3), as the efficiency of scattering into the 992 cm^{-1} mode after IVR (which must therefore be HL) is reduced. Indeed, it has been shown that the effective radiative lifetime for emission into the 992 cm^{-1} mode (as well as the ν_1 overtones and $2\nu_6 + n\nu_1$ progression members) after IVR will be T_1/N .⁵²⁻⁵⁴ Therefore, the ratio of HL/RRS intensity predicted by Eq. (3) is close to unity if the value of N were near 20-30.

Parmenter *et al.*⁵³ have noted in their para-difluorobenzene studies that once the existence of a dynamic IVR has been established, the relative amounts of structured and unstructured emission observed in the collision-free emission spectrum can be used as a general guide in determining the likelihood of whether "intermediate" case ($N < 30$) or statistical case ($N > 30$) IVR dynamics will be observed. A comparison of their collision free para-difluorobenzene spectra to the series of emission spectra from 6^11^n levels ($n \leq 5$) in benzene obtained by Yoshihara under similar experimental conditions reveals that the 6^11^5 level indeed appears to be a borderline intermediate-statistical case IVR. This suggests an N value around 30 for the 6^11^5 vibronic level and further supports our conclusions concerning the role of a high density of background states in determining whether RRS or HL components of the resonant light scattering process will be manifested in the isolated benzene molecule.

VI. SUMMARY AND CONCLUSIONS

We have measured the absolute scattering cross section of the 992 cm^{-1} Raman active mode of benzene in the vapor phase as excitation moves through the $6^1_01^5_0$ vibronic absorption band $\sim 5100\text{ cm}^{-1}$ above the ${}^1B_{2u}$ origin. Structured emission from the 6^11^5 level is clearly observed with excitation in resonance with this absorption band in the form of an enhanced intensity in ν_1 992 cm^{-1} fundamental and the spectral appearance of the ν_1 overtones as well as a progression in $2\nu_6 + n\nu_1$. By means of an excitation profile analysis of the 992 cm^{-1} fundamental, we have distinguished between resonance Raman scattering and hot luminescence components of the resonant light scattering process. We find that the observed 992 cm^{-1} excitation profile reflects both of these components. Therefore, the structured emission from the high energy short lived ${}^1B_{2u}$ vibronic states studied here cannot be termed simply as hot luminescence or single vibrational level fluorescence as is common in the literature since a significant component of this structured emission is rigorously resonance Raman scattering.

An interference pattern in the resonance Raman com-

ponent of the 992 cm^{-1} excitation profile deriving from the interference between the resonant ${}^1B_{2u}$ Raman amplitude and the preresonant Raman amplitude from higher energy electronic states demonstrates that some molecules in the ensemble are scattering from a virtual or superposition state where the summation over all excited states in the Kramers–Heisenberg expression for the molecular Raman polarizability is still valid. However, the HL component of the 992 cm^{-1} resonance emission occurs independently of the 992 cm^{-1} scattering amplitude contributed by the higher energy electronic states. The HL derives from different molecules which have populated isoenergetic ${}^1B_{2u}$ molecular eigenstates prior to emission of the photon.

In our experiments, the process responsible for the destruction or dephasing of the superposition state, which facilitates population of isoenergetic ${}^1B_{2u}$ molecular eigenstates, is dynamic intramolecular vibrational redistribution rather than the pseudoelastic collisions normally associated with pure-dephasing effects in the vapor phase. The IVR process simply reflects the statistical effects of a high density of background states within the molecule which provide a bath for dephasing the states being coupled by the incident field. Prior to IVR, RRS will occur, while after IVR only HL will be observed from the populated ${}^1B_{2u}$ molecular eigenstates.

ACKNOWLEDGMENTS

We would like to thank Dr. C. R. Johnson for helpful discussions and assistance in the early stages of this work. We gratefully acknowledge partial support of this work from NIH Grant No. 1R01-GM30741-06. Sanford A. Asher is an Established Investigator of the American Heart Association; this work was done during the tenure of an Established Investigatorship of the American Heart Association and with funds contributed in part by the American Heart Association, Pennsylvania affiliate.

- ¹D. L. Rousseau and P. F. Williams, *J. Chem. Phys.* **64**, 3519 (1976); D. L. Rousseau, P. F. Williams, and D. Woretsky, *Phys. Rev. Lett.* **32**, 196 (1974).
²N. Bloembergen, H. Lotem, and R. T. Lynch, Jr., *Ind. J. Pure Appl. Phys.* **16**, 151 (1978).
³Y. Prior, A. R. Bogdan, M. Degenais, and N. Bloembergen, *Phys. Rev. Lett.* **46**, 111 (1981).
⁴N. Bloembergen, *Nonlinear Optics*, edited by W. P. Benjamin (Benjamin, Reading, 1977).
⁵S. Mukamel, *Phys. Rev. A* **28**, 3408 (1983).
⁶Y. R. Shen, *Phys. Rev. B* **9**, 622 (1974).
⁷K. E. Jones and A. H. Zewail, *Advances in Laser Chemistry*, edited by A. H. Zewail (Springer, Berlin, 1978), p. 196.
⁸A. Nitzan, *Chem. Phys.* **41**, 163 (1979).
⁹D. L. Huber, *Phys. Rev.* **158**, 843 (1967); **170**, 418 (1968).
¹⁰R. M. Hochstrasser and C. A. Nyi, *J. Chem. Phys.* **70**, 1112 (1979).
¹¹J. L. Carlsten and A. Szoke, *Phys. Rev. Lett.* **36**, 1667 (1976).
¹²F. A. Novak, J. M. Friedman, and R. M. Hochstrasser, *Laser Coherence Spectroscopy*, edited by J. I. Steinfield (Plenum, New York, 1980).

- ¹³D. Lee and A. C. Albrecht, *Advances in Infrared and Raman Spectroscopy*, edited by R. J. H. Clark and R. E. Hester (Wiley–Heyden, New York, 1985), p. 179.
¹⁴S. Mukamel, *J. Chem. Phys.* **82**, 5399 (1985).
¹⁵A. E. W. Knight, C. S. Parmenter, and M. W. Schuyler, *J. Am. Chem. Soc.* **97**, 1993, 2005 (1975).
¹⁶T. A. Stephenson, P. L. Radloff, and S. A. Rice, *J. Chem. Phys.* **81**, 1060 (1984).
¹⁷J. M. Freidman and R. M. Hochstrasser, *Chem. Phys.* **6**, 155 (1974).
¹⁸D. O. Conner, M. Sumitani, Y. Takagi, N. Nakashima, K. Kamogawa, Y. Udagawa, and K. Yoshihara, *J. Phys. Chem.* **87**, 4848 (1983).
¹⁹J. Behringer, *J. Raman Spectrosc.* **2**, 275 (1974).
²⁰B. Hudson and L. D. Ziegler, *J. Phys. Chem.* **88**, 1110 (1984).
²¹M. Sumitani, D. O. Conner, Y. Takagi, N. Nakashima, K. Kamogawa, Y. Udagawa, and K. Yoshihara, *J. Chem. Phys.* **13**, 359 (1985).
²²M. Sumitani, D. O. Conner, Y. Takagi, N. Nakashima, K. Kamogawa, Y. Udagawa, and K. Yoshihara, *Chem. Phys. Lett.* **97**, 508 (1983).
²³H. J. Neusser, L. Wunsch, and E. W. Schlag, *Z. Naturforsch. Teil A* **36**, 1340 (1981).
²⁴E. Riedle and H. J. Neusser, *J. Chem. Phys.* **80**, 4648 (1984).
²⁵E. Riedle, H. J. Neusser, and E. W. Schlag, *J. Phys. Chem.* **86**, 4848 (1982).
²⁶D. B. Moss and C. S. Parmenter, *J. Phys. Chem.* **90**, 1011 (1986).
²⁷E. Riedle, H. J. Neusser, and E. W. Schlag, *J. Phys. Chem.* **88**, 198 (1984).
²⁸T. A. Stephenson and S. A. Rice, *J. Chem. Phys.* **73**, 4765 (1980).
²⁹K. G. Spears and S. A. Rice, *J. Chem. Phys.* **55**, 5561 (1971).
³⁰M. W. Schuyler and C. S. Parmenter, *Trans. Nonrad. Mol., Reun. Soc. Chem. Phys.* **20**, 92 (1970) (Supp. to *J. Chem. Phys.*).
³¹R. Lopez-Delgado, J. E. Parkin, and J. H. Callomon, *Chem. Phys. Lett.* **13**, 125 (1972).
³²C. R. Johnson and S. A. Asher, *J. Phys. Chem.* **89**, 1375 (1985).
³³P. A. Harmon and S. A. Asher, *J. Phys. Chem.* (to be submitted).
³⁴S. A. Asher, C. R. Johnson, and J. Murtaugh, *Rev. Sci. Instrum.* **54**, 1657 (1983).
³⁵G. Black and W. K. Bischel, in *Excimer Lasers*, edited by C. K. Rhodes, H. Egger, and H. Pummer (American Institute of Physics, New York, 1983).
³⁶G. H. Atkinson and C. S. Parmenter, *J. Mol. Spectrosc.* **73**, 20 (1978).
³⁷J. H. Callomon, T. M. Dunn, and I. M. Mills, *Philos. Trans. R. Soc. London Ser. A* **259**, 499 (1966).
³⁸W. F. Radle and C. A. Beck, *J. Chem. Phys.* **8**, 507 (1940).
³⁹G. H. Atkinson and C. S. Parmenter, *J. Phys. Chem.* **75**, 1564 (1971).
⁴⁰S. M. Beck, M. G. Liverman, D. L. Montis, and R. E. Smalley, *J. Chem. Phys.* **70**, 232 (1979).
⁴¹D. P. Craig, *J. Chem. Soc.*, **1950**, 2146.
⁴²E. F. McCoy and E. G. Ross, *Aust. J. Chem.* **15**, 573 (1962).
⁴³R. Mathies, *Biol. Appl. Reson. Raman Spectrosc.* (to be published).
⁴⁴See, for example, J. Tang and A. C. Albrecht, *Raman Spectroscopy, Theory and Practice*, edited by H. A. Szymanski (Plenum, NY, 1970), Vol. II.
⁴⁵J. Friedman and R. Hochstrasser, *Chem. Phys. Lett.* **32**, 414 (1975).
⁴⁶P. Stein, V. Misowski, W. Woodruff, J. Griffin, K. Werner, B. Gaber, and T. Spiro, *J. Chem. Phys.* **64**, 2159 (1976).
⁴⁷T. Oka, *Adv. At. Mol. Phys.* **9**, 127, (1973).
⁴⁸R. A. Coveleskie and C. S. Parmenter, *J. Chem. Phys.* **69**, 1044 (1978).
⁴⁹C. S. Parmenter and K. Y. Tang, *Chem. Phys.* **27**, 127 (1978).
⁵⁰S. H. Kable, J. W. Thoman, Jr., S. Beames, and A. E. W. Knight, *J. Phys. Chem.* **91**, 1004 (1987).
⁵¹G. M. Stewart and J. D. McDonald, *J. Chem. Phys.* **76**, 5637 (1982).
⁵²K. F. Freed and A. Nitzan, *J. Chem. Phys.* **73**, 4765 (1980).
⁵³See, for example, (a) C. S. Parmenter, *J. Phys. Chem.* **86**, 1735 (1982); (b) R. A. Coveleskie, D. A. Dolson, and C. S. Parmenter *ibid.* **89**, 645, 655 (1985); (c) K. W. Holtzclaw and C. S. Parmenter *J. Chem. Phys.* **84**, 1099 (1986); (d) D. A. Dolson, K. W. Holtzclaw, D. B. Moss, and C. S. Parmenter, *J. Chem. Phys.* **84**, 1119 (1986).
⁵⁴S. Mukamel, *J. Chem. Phys.* **82**, 2867 (1985).